Electronic Supplementary Material (ESI) for CrystEngComm.

Supplementary Information

Precursor Purity Effects on Solution-Based Growth of $MAPbBr_3$ Single Crystals towards Efficient Radiation Sensing

Jeremy T. Tisdale[*,1], Travis Smith*[*,2], John Robert Salasin[1], Mahshid Ahmadi[1], Nathan Johnson[2], Anton V. Ievlev[3], Michael Koehler[1], Claudia J. Rawn[1], Eric Lukosi[2] and Bin Hu[1]*

[1]Department of Materials Science and Engineering, University of Tennessee-Knoxville, Tennessee 37996-4545, USA

[2]Department of Nuclear Engineering, University of Tennessee-Knoxville, Tennessee 37996-4545, USA

[3]Center for Nanophase Materials Sciences, Oak Ridge National Laboratory, Oak Ridge, Tennessee 37831-6056, USA

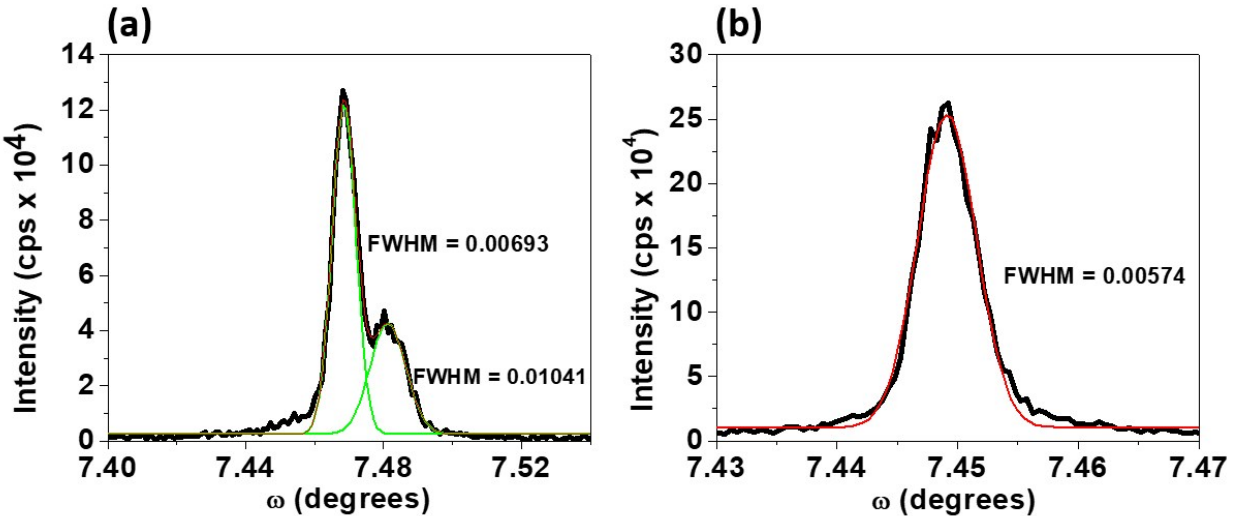

Figure S1. Triple axis rocking curves for (a) low purity and (b) high purity $MAPbBr_3$ single crystals.

Figure S1 shows the triple axis rocking curves for low and high purity single crystals of $MAPbBr_3$. The FWHM values of the peaks of the rocking curves directly measures the mosaicity and long-range order of crystallites. To compare the FWHM values between high and low purity samples, the first peak of the low purity (FWHM = 0.00693) is broader than the peak of high purity (FWHM = 0.00574). This shows that there is more disorder in the low purity $MAPbBr_3$ single crystal. Also, the high purity sample is a symmetric curve, alluding to high crystalline quality, whereas the low purity rocking curve is asymmetrical with the presence of the second small peak. The second small peak is broader (FWHM = 0.01041) and alludes to plane tilting in the low purity sample.

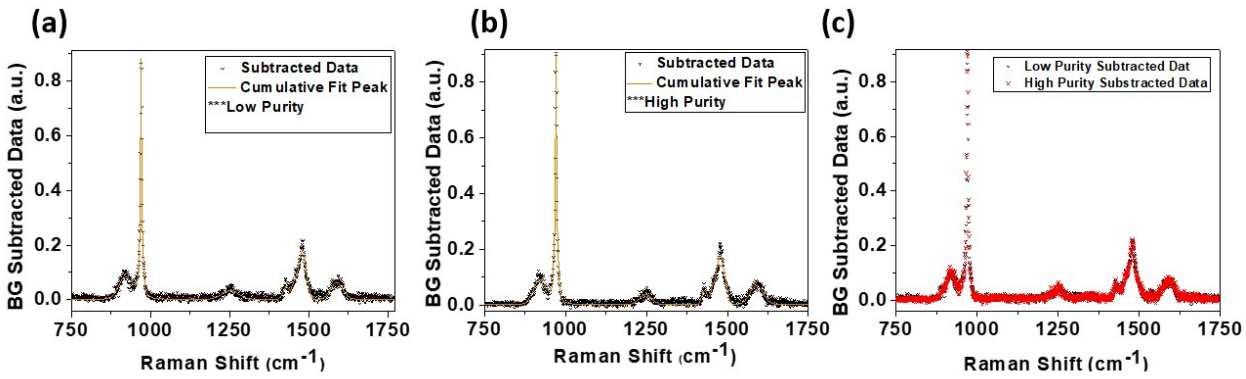

Figure S2. Raman spectroscopy fitting for (a) low purity, (b) high purity and (c) comparison plot for both fitted data sets.

Figure S2 shows the fitting plots for Raman spectroscopy data taken for low and high purity $MAPbBr_3$ single crystals. Table S1 below shows the fitting parameters for peak position, peak height, and peak area for quantitative comparison between the two samples.

Table S1. Raman spectroscopy fitting data for peak position, height and area for low and high purity $MAPbBr_3$ single crystals.

Purity	Position (cm^{-1})	Height	Area
High	920.5	0.087	4.25
Low	921.2	0.078	4.32
High	970.4	0.902	8.31
Low	970.3	0.876	8.10
High	1248.5	0.036	1.67
Low	1251.9	0.032	2.06
High	1429.4	0.051	1.04
Low	1428.9	0.049	1.13
High	1453.3	0.044	0.70
Low	1453.2	0.047	0.81
High	1478.7	0.180	5.63
Low	1478.9	0.180	5.51
High	1590.3	0.067	3.43
Low	1588.7	0.061	3.00

In Table S1, minimal differences are observed between the Raman peak positions, height and area with an average difference between high and low purity of 0.94 cm^{-1} in peak position, 0.0071 in peak height and 0.20 in peak area. These small variations may be attributed to experimental error, as no large differences are observed in any of the peaks. This shows that both samples have similar organic vibrational modes, showing that no large impurities are incorporated into the crystal structure that would affect the local structure when using low or high purity precursors.

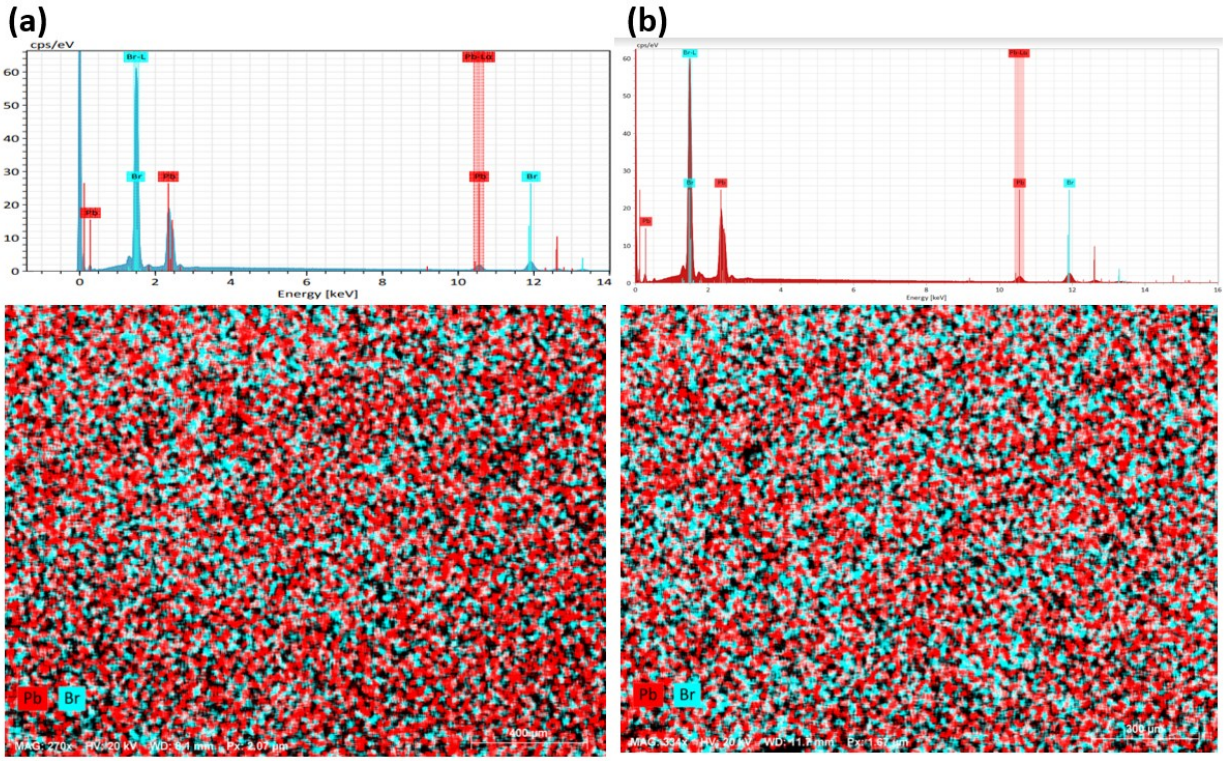

Figure S3. EDS energy spectra and map for Pb and Br content for (a) low purity $MAPbBr_3$ and (b) high purity $MAPbBr_3$ single crystals.

Figure S3 shows EDS maps and energy spectra for low and high purity $MAPbBr_3$ single crystals. Here, it is observed that the Pb to Br content ration is 1:3 and homogeneous across the surface of the samples regardless of crystallite size and disorder. This demonstrates homogeneity of $MAPbBr_3$ with no large impurities that would affect the ratio of Pb to Br. Organic composition is furthered explored via ToF-SIMS as EDS is not sufficient for low-Z elemental analysis.

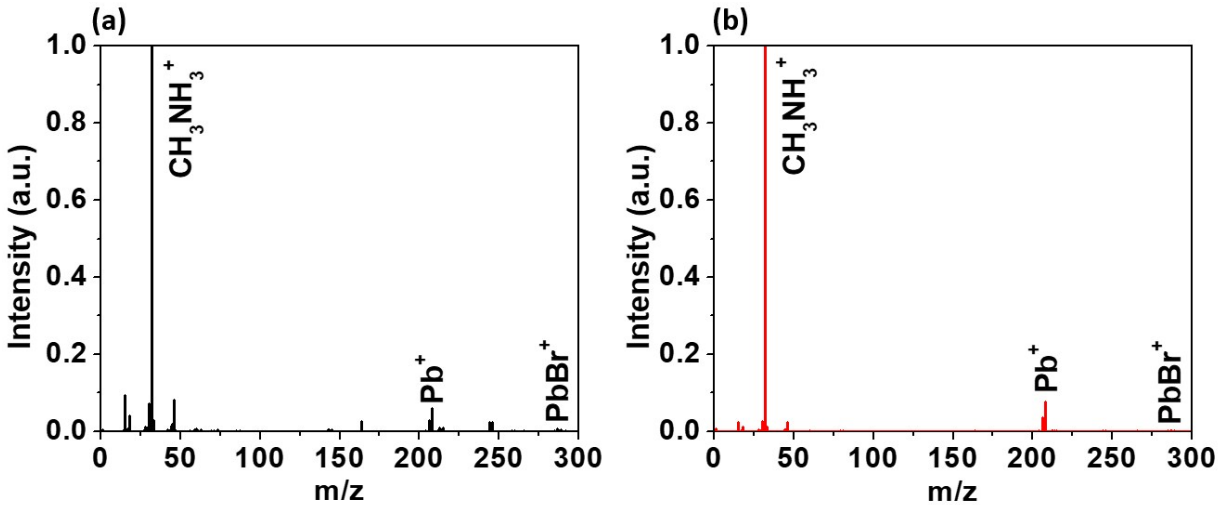

Figure S4. ToF-SIMS for $MAPbBr_3$ single crystals (key peaks labeled) showing the (a) 98%-based depth profile and (b) high purity depth profile. A Cs beam was used for the measurement; therefore, the Cs peak was removed for analysis.

ToF-SIMS positive ion mass spectrometry spectra are shown for $MAPbBr_3$ single crystals with low purity and high purity precursors in Figure S4a and S4b, respectively. For each sample, three key peaks were identified as $CH_3NH_3^+$ (m/z = 32.05), Pb^+ (m/z = 208.98), and $PbBr^+$ (m/z = 286.89). Smaller peaks around $CH_3NH_3^+$ were identified as other organic compounds, such as CH_2^+ (m/z = 14.02) at lower values, and up to $C_3H_9N_2^+$ (m/z = 73.05) at higher values. Br^+ (m/z = 78.92) and $^{81}Br^+$ (m/z = 80.92) were also identified in each spectrum. We attribute the low-intensity peaks to loosely bonded compounds in the $MAPbBr_3$ single crystals such as organic components bonded with Pb^+ or Br^+. Comparing the two ToF-SIMS spectra, there are small differences between the two precursor purities in elemental composition. However, the ToF-SIMS software analysis only identified the peaks of MA^+, Pb^+ and $PbBr^+$, suggesting that impurities from lower purity precursors are not incorporated into the perovskite crystal structure when $MAPbBr_3$ single crystals are grown via ITC method. Other small peaks observed in the low purity samples may be attributed to the regions with poor alignment of nano-sized crystallites. We propose that low impurity samples are grown, regardless of purity of precursors, due to solution-based crystal

growth and stringent requirements for inclusions in the perovskite crystal structure. Unlike melt growths or solid growths, where any impurity in the stock material is incorporated into the final crystalline material, solution-based growth allows for impurities to be removed via filtering of the solution before growth and have less impurities incorporated through crystallization as impurities are left behind in the excess solution as the single crystalline $MAPbBr_3$ forms. This process is similar to purification of materials via recrystallization.

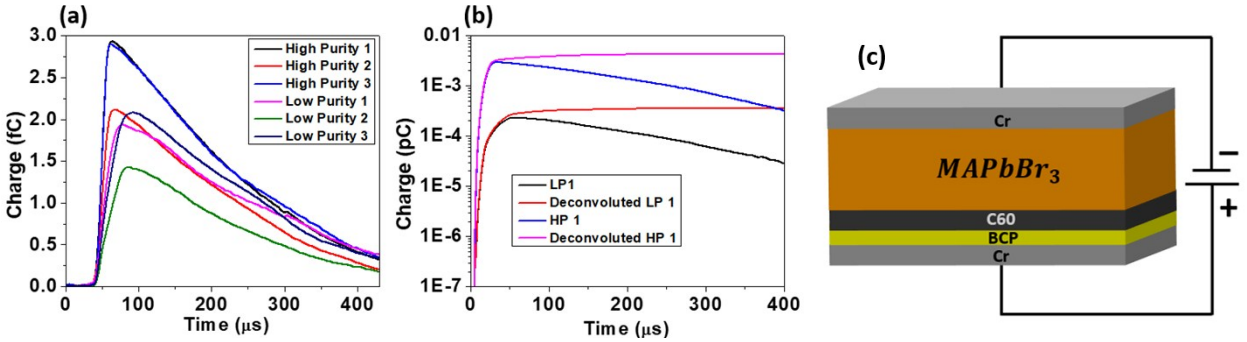

Figure S5. Preamplifier output pulse for both (a) low purity (LP) and (b) high purity (HP) based radiation detectors. (c) Shows schematic for device structure used during alpha radiation sensing and rise time measurements.

Figure S5a shows the averaged preamplifier transient signals used for mobility calculations to compare charge carrier properties between different purities used for $MAPbBr_3$ radiation sensing devices. Devices were exposed to alpha particles from a ^{210}Po source and the pulse shape was recorded using an oscilloscope. We estimated the mobility for each detector assuming a flat electric field and compared charge collection via pulse height. The data is shown in Table S2. The drift mobility for each detector is similar, showing it is not affected by precursor purity. In Figure S5b, the rise time signals are deconvoluted to remove ballistic deficit from the decay of the preamplifier to compare the amount of charge collection in the detectors. More charge is collected in the high

purity samples, which we attribute to less charge trapping due to reduced impact from crystallite boundary defect sites.

Table S2. Mobility ($^{cm^2}/_{V*s}$) estimations and statistical data for high and low purity detectors.

Sample	Thickness (mm)	H_0 (Channel number)	Resolution (%)	Rise time (μs)	Mobility ($cm^2/V/s$)
LP 1	1.9406 ± 0.0025	77	26.0	17.5 ± 0.7	17.9 ± 0.7
LP 2	2.0853 ± 0.0025	94	11.7	20.5 ± 0.8	17.7 ± 0.7
LP 3	2.0218 ± 0.0025	108	16.7	23.6 ± 0.9	14.4 ± 0.6
HP 1	1.4935 ± 0.0025	118	19.89	10.1 ± 0.4	18.4 ± 0.8
HP 2	1.5951 ± 0.0025	172	16.3	11.3 ± 0.5	18.9 ± 0.8
HP 3	1.3183 ± 0.0025	208	18.3	9.5 ± 0.4	15.3 ± 0.6